NUMERICAL SIMULATION OF UNSTEADY FLOW AT PO RIVER DELTA

By D. Ambrosi,[1] S. Corti,[2] V. Pennati,[3] and F. Saleri[4]

ABSTRACT: This paper describes a numerical simulation of the flow at the delta of the Po River, the main Italian river. We take into account a portion of the river that is 20 km long, characterized by a complex geometry consisting of narrow bends and strong gradients in the profile of the riverbed. To account for the presence of tidal effects, a nonstationary solution is sought. The considered model consists in the classical two-dimensional (2D) Saint-Venant equations, written in conservation form. This system of partial differential equations is discretized by a finite-element scheme that has some particularly attractive features for river flow. The accuracy of the scheme is verified on a few test cases, then a numerical simulation of the flow of the Po over three days is implemented. The numerical results are then compared with the experimental measures and discussed in the light of the assumptions made in the construction of the model.

INTRODUCTION

The Po River is both the longest Italian River and the one with largest discharge, so that the study and, possibly, prediction of its flow is an obvious major goal. The Italian Energy Supply Comission (ENEL) has always had an interest in the simulation of flows in rivers and basins. In particular, the presence of a power station in the vicinity of the delta of the Po River makes the simulation of the flow in this region desirable. ENEL has carried out, over many years, a large number of experimental measures for this purpose.

To carry out a numerical simulation of the flow at the Po delta, in the present work, we consider the classical shallow-water model (SWE) and its integration by a finite-element scheme. The finite-element method, although not as popular as finite differences, has already been used for the numerical integration of the shallow-water equations by several researchers; some of the approaches are described in Lynch and Gray (1979), Di Monaco and Molinaro (1988), and Leclerc et al. (1990). These approaches differ mainly in the choice of a time-advancing scheme ranging from a Newton-Raphson linearization of the whole system to a reformulation of the differential problem in terms of a generalized wave equation that replaces the continuity equation. The time-advancing method adopted here is of fractional step type and closely resembles the scheme proposed by Benquè et al. (1982), using the finite-difference technique. Here it is revisited in a finite-element framework. The main idea underlying this formulation is the splitting, at every time step, of the equations of the differential system to decouple the physical contributions. In particular, the wave traveling at speed $\sqrt{gh}$, which is the most restrictive with respect to the maximum time step allowed in this kind of problem, is treated implicitly with a low computational cost. In the discussion of the numerical results, it will be shown that this method, coupled with a Lagrangian treatment of the convective terms, totally avoids the oscillations for the velocity that are known to plague the finite-element approximations of the shallow-water equations written in primitive form (Westerink et al. 1994; Walters 1983).

One of the aims of the present work is to check the degree of confidence one can have in a two-dimensional (2D) model for the simulation of a real unsteady river flow with a complex delta and riverbed profile. This geometry of the Po River is well known and measures for the bottom depth, elevation, and unit-width discharge are available. The limitations of the shallow-water model in this particular simulation are well known, such as the poor resolution of the dynamics of the bottom friction. However, the practical efficiency of this model has been highlighted by the good correspondence obtained between numerical and experimental results. This is achieved by using a robust time-advancing scheme in the numerical model. An additional motivation for the study of a 2D model is the evident savings in computational cost; in particular, a three-dimensional (3D) code expected to solve a real unsteady flow on a parallel architecture relies on a 2D model, which can run efficiently on a workstation in a few hours. In the final section, we will discuss the computational efficiency of this approach.

SHALLOW-WATER EQUATIONS

SWE in conservative differential form reads (Cunge et al. 1981)

$$\frac{\partial \mathbf{q}}{\partial t} + \nabla\cdot(\mathbf{q}\mathbf{q}/h) - \nabla\cdot(\mu\nabla\mathbf{q}) + gh\nabla\xi = -g\frac{\mathbf{q}|\mathbf{q}|}{h^2h^{1/3}K^2} - 2\Omega\times\mathbf{q} \tag{1}$$

$$\frac{\partial \xi}{\partial t} + \nabla\cdot\mathbf{q} = 0 \tag{2}$$

where $\mathbf{q}(x, y, t) = (q_x, q_y)^T$ = unit-width discharge; ξ = elevation over a reference plane; h = total depth of the water; μ = dispersion coefficient; g = gravity acceleration; Ω = angular velocity of the earth; and K = Strickler coefficient. A schematic representation of some of these quantities may be seen in Fig. 1.

According to the theory of characteristics, if $\mu = 0$ and the

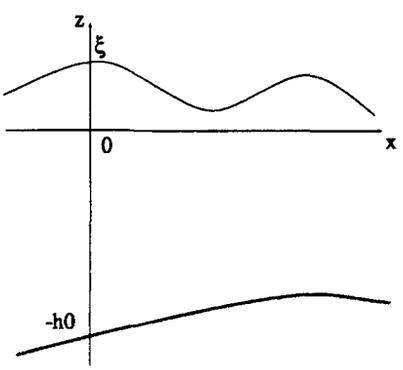

FIG. 1. Elevation and Depth

[1]Res., Ctr. for Res., Devel., and Advanced Studies in Sardinia (CRS4), Via Nazario Sauro, 10, 09123, Cagliari, Italy.
[2]Res., ENEL-DSR-CRIS, Via Ornato 90/14, 20162, Milano, Italy.
[3]Res., ENEL-DSR-CRIS, Via Ornato 90/14, 20162, Milano, Italy.
[4]Res., Politecnico di Milano, P.le Leonardo da Vinci 32, 20133, Milano, Italy.

Note. Discussion open until May 1, 1997. To extend the closing date one month, a written request must be filed with the ASCE Manager of Journals. The manuscript for this paper was submitted for review and possible publication on November 28, 1994. This paper is part of the ***Journal of Hydraulic Engineering***, Vol. 122, No. 12, December, 1996. ISSN 0733-9429/96/0012-0735–0743/$4.00 + $.50 per page. Paper No. 9672.

flow is subcritical, two boundary conditions are to be prescribed at the inflow and one at the outflow. However, when considering the case $\mu \neq 0$, the presence of the diffusion term in system (1) and (2) requires the imposition of a proper boundary condition for the unit-width discharge on the whole boundary and, moreover, as μ is usually very small in the applications, it is natural to require that these boundary conditions recall the inviscid case as the viscosity coefficient tends to zero. Therefore, the boundary conditions applied here are as follows: prescribe as many Dirichlet conditions as are required by the characteristic theory, plus one Neumann boundary condition for each component of the unit-width discharge where its value is not yet imposed (Oliger and Sundstrom 1978). Note that the weak Neumann condition on $\mathbf{q}$ arises naturally in the integration by parts of the diffusive term, when considering the weak form of (1).

NUMERICAL SCHEME

The main idea behind the adopted time-advancing scheme is to split the equations at every time step to decouple the physical contributions. The discretization in time of the system (1) and (2) leads to the following equations to be solved:

Step 1

$$\mathbf{v}^n = \mathbf{q}^n/h^n; \quad \mathbf{v}^{n+1/3} = \mathbf{v}^n \bigcirc \mathbf{X} \tag{3}$$

Step 2

$$\mathbf{q}^{n+1/3} = h^n\mathbf{v}^{n+1/3}; \quad \mathbf{q}^{n+2/3} + \Delta t g \frac{\mathbf{q}^{n+2/3}|\mathbf{q}^{n+1/3}|}{h^2h^{1/3}K^2} = \mathbf{q}^{n+1/3} + \Delta t[\nabla\cdot(\mu\nabla\mathbf{q}^{n+1/3}) - 2\Omega \times \mathbf{q}^{n+1/3}] \tag{4}$$

Step 3

$$\mathbf{q}^{n+1} - \mathbf{q}^{n+2/3} + \Delta t g h^n \nabla\xi^{n+1} - \frac{\mathbf{q}^{n+2/3}}{h^n}(\xi^{n+1} - \xi^n) = 0 \tag{5}$$

$$\xi^{n+1} - \xi^n + \Delta t \nabla\cdot\mathbf{q}^{n+1} = 0 \tag{6}$$

The symbol $\mathbf{v}^n \bigcirc \mathbf{X}$ indicates the value of the velocity obtained by a Lagrangian integration, using the method discussed in the following section. At the third step, (5) and (6) are decoupled by subtracting the divergence of (5) from (6). One then solves the following Helmholtz-type equation:

$$\xi^{n+1} - (\Delta t)^2\nabla\cdot(gh^n\nabla\xi^{n+1}) + \Delta t\nabla\cdot\left(\frac{\mathbf{q}^{n+2/3}}{h^n}\xi^{n+1}\right) = \xi^n - \Delta t\nabla\cdot\mathbf{q}^{n+2/3} + \Delta t\nabla\cdot\left(\frac{\mathbf{q}^{n+2/3}}{h^n}\xi^n\right) \tag{7}$$

This new elevation is then used to solve (5).

The spatial discretization of (4)–(6) is based on the Galerkin finite-element method; the basic theory of the Galerkin approach may be found, for example, in Zienkiewikz and Taylor (1989), Quarteroni and Valli (1994) and, particularly referring to SWE, in Agoshkov et al. (1993). The weak formulation of (3)–(6) is accomplished in a standard way and is not shown here. An important aspect of the spatial discretization of (4)–(7) is that two different spaces of representation have been used for the unknowns: the elevation is interpolated by P1 functions, and the unit-width discharge is interpolated by P2 functions. As usual, P1 is the set of piecewise linear functions on triangles; P2 is the set of piecewise quadratic functions on triangles. The choice of these interpolation spaces, first suggested in Walters (1983), eliminates the spurious oscillations that arise in the elevation field when a P1-P1 representation is used. To our knowledge, no theoretical explanation of incompatibility between spaces of representation of the unknowns has yet been stated theoretically for SWE.

The main advantage of this fractional-step procedure is that the wave traveling at speed $\sqrt{gh}$ is decoupled in the equations and treated implicitly. Therefore, the Courant-Friedrichs-Lewy condition due to the celerity is cheaply circumvented. Moreover, as the Lagrangian integration is unconditionally stable and all the terms appearing in (4) are discretized implicitly, the resulting scheme is unconditionally stable.

A drawback of a fractional-step scheme, as the one adopted here, is that this scheme is only first-order accurate in time. However, this is not an actual disadvantage as the model deals with tidal phenomena that vary slowly in time. From a mathematical point of view, in this fractional-step framework, one requires, a priori, that the boundary conditions to be satisfied by the collection of fractional steps coincide with the boundary conditions to be satisfied by the original differential system, as described previously. Unfortunately, at step 3 the solution of the elliptic in (7) requires the imposition of proper boundary conditions for the elevation on the whole boundary and, in the practical applications, this may not be the case. To overcome this difficulty, we relax the original requirement, and at this

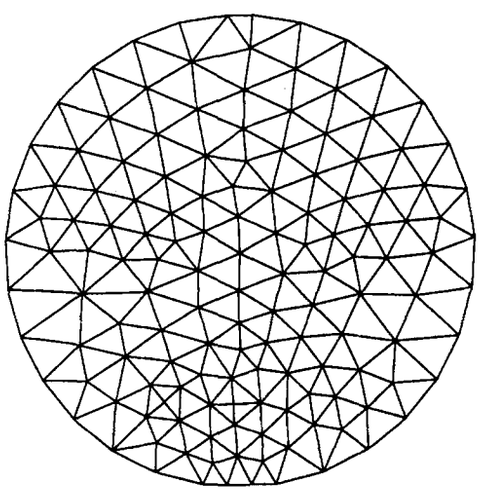

FIG. 2. Jet Circulation in Reservoir—Computational Mesh

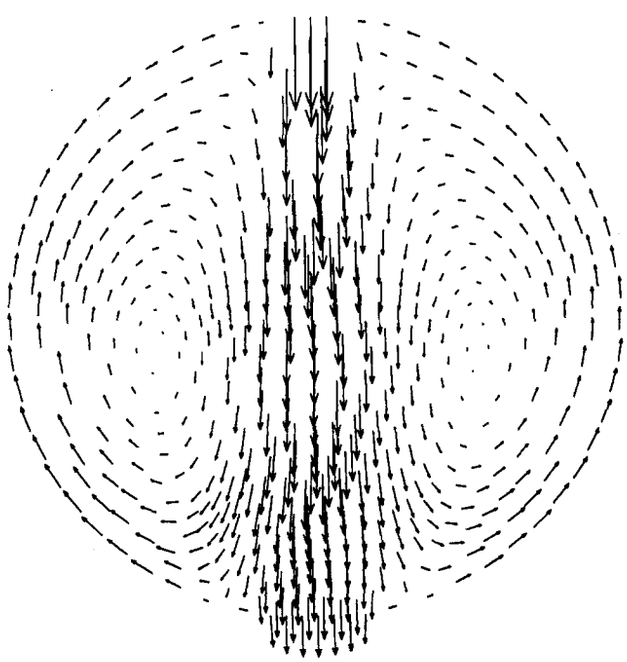

FIG. 3. Jet Circulation in Reservoir—Velocity Field

step we impose a Neumann condition on the part of the boundary where the value of the elevation is not originally given. In the test cases, one can observe that this procedure works well in practice.

In the integration of the weak formulation of (4) and (5), the lumping technique has been adopted for the mass matrices of **q**. By the term "mass lumping," we intend the use of a low-order quadrature formula for the evaluation of the integrals involving the nondifferential terms, yielding a diagonal stiffness mass matrix. It is well known that for P2 elements a nontrivial diagonalization has to be performed (as may be the case of P1); otherwise a singular matrix is recovered [see Appendix 8 in Zienkiewikz and Taylor (1989)]. This difficulty has been overcome in the following way. Each triangle of the mesh is divided into four parts by connecting the midpoints of the sides; it is then possible to use the three vertex-points rule on each subtriangle. The total integral is then the sum of the subintegrals and automatically leads to a diagonal mass matrix.

A possible objection to this approach is that the mass-lumping technique is known to produce large phase errors for unsteady problems, which are precisely the ones we are interested in. However, at step 2 no wave-type phenomena are involved, and the dissipation coefficient is usually so small that the diffusive term can be treated explicitly without resulting in any additional unphysical constraints. On the other hand, when considering (5) for given ξ^{n+1}, the equation is explicit.

The computational effort required by this scheme for the solution of algebraic systems therefore consists of the inversion of one symmetric matrix, with size coinciding with the number of P1 nodes.

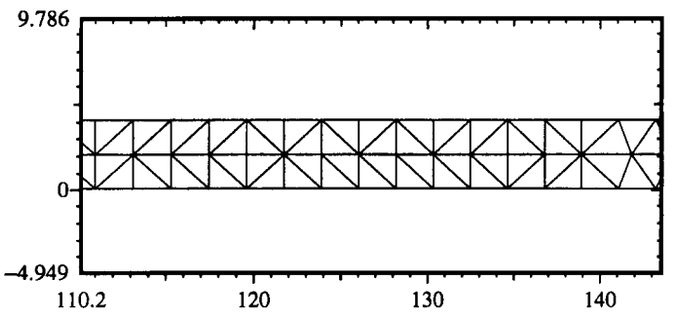

FIG. 4. Detail of Regular Mesh Used in Test Case 2

Lagrangian Scheme for Convective Terms

At step 1, the advective part of the momentum equation is integrated by a Lagrangian scheme (Benquè et al. 1982; Pironneau 1982). Rewriting the convective terms of (1) in Lagrangian form results in the solution of two, coupled, ordinary differential equations

$$d\mathbf{v}[\mathbf{X}(t), t]/dt = 0 \tag{8}$$

$$d\mathbf{X}/dt = \mathbf{v}[\mathbf{X}(t), t] \tag{9}$$

The curve $\mathbf{X}(t)$ is the characteristic line, and its slope is the velocity itself so that, at this stage, it coincides with the pathline. The velocity field plays a double role: it is the unknown to be determined as well as the slope of the characteristic curve. As we are interested in computing the solution at the nodes of the mesh, let us consider the node with coordinates **y**. The initial condition associated with (9) must be

$$\mathbf{X}(t^{n+1}) = \mathbf{y} \tag{10}$$

To integrate (9), we need to know the slope of the characteristic curve at **y** at time t^{n+1}, which is unfortunately the unknown velocity itself. Therefore, the slope of the characteristic line has to be approximated in some way, for instance by a zero-order extrapolation in time. Assuming the use of a second-order Runge-Kutta scheme to integrate (9), the algorithm is as follows:

$$\tilde{\mathbf{X}} = \mathbf{y} - \frac{\Delta t}{2}\mathbf{v}^n(\mathbf{y}) \tag{11}$$

$$\mathbf{X}(t^n) = \mathbf{y} - \Delta t\mathbf{v}^n(\tilde{\mathbf{X}}) \tag{12}$$

and (8) immediately gives

$$\mathbf{v}^{n+1/3}(\mathbf{y}) = \mathbf{v}[\mathbf{X}(t^{n+1}), t^{n+1}] = \mathbf{v}[\mathbf{X}(t^n), t^n] \tag{13}$$

As the Lagrangian integration requires the primitive form of the equations, the fourth term that appears on the left side of (5) has been added to ensure consistency with (1), which is written in conservation form. We note that, apart from this

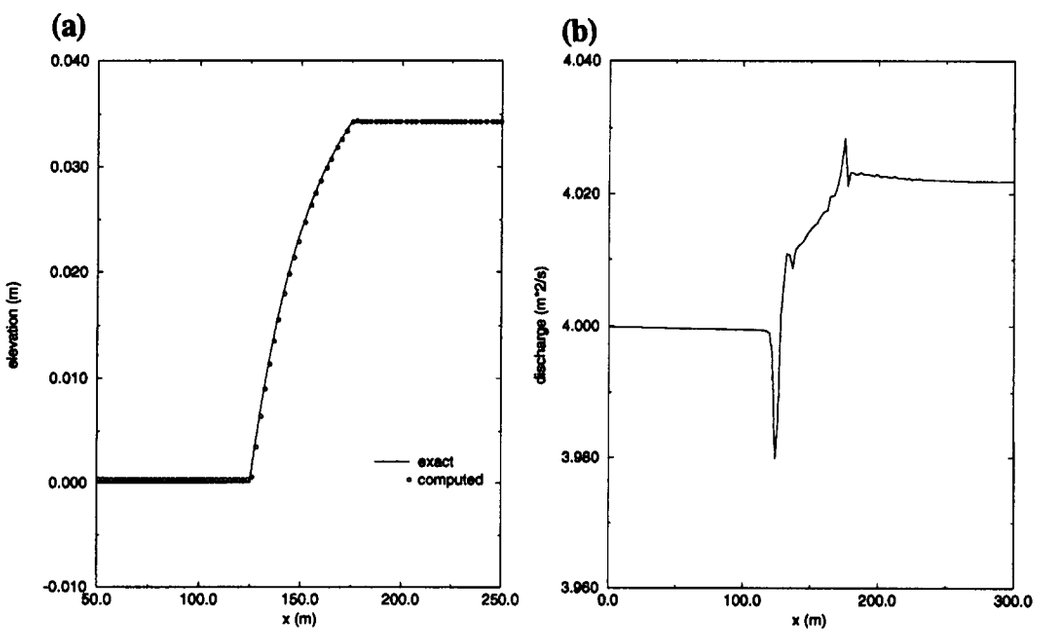

FIG. 5. Water Elevation and Unit-Width Discharge for 1D Test Case

term, the discrete counterpart of (3)–(6) requires the inversion of symmetric matrices only. However, this consistency term is of minor relevance in all the flows in which the typical time scale is much larger than the time step (as is the case of tides). Therefore, the usual conjugate gradient algorithm can be confidently used in this kind of simulation.

The Lagrangian discretization of the transport terms has many attractive features: it avoids spurious oscillations arising due to the centered treatment without the inclusion of any nonphysical viscosity coefficients and it eliminates any restrictions on the time step. However, when using unstructured grids, the pathline reconstruction requires the knowledge of the element in which the foot of the pathline falls. This research consists of a greater algorithmic effort than that on structured grids. In practice, this difficulty has been overcome in the code by defining an ordered list containing all the elements that are adjacent to a node or to a given element. In this way, the search for the element in which the pathline foot falls is restricted to clusters of elements. To avoid that the foot of the reconstructed pathline falls outside of the domain, the rigid boundary of the domain is always assumed to be a stream line.

It is worthwhile to remark that the quadratic representation of velocities, that has been adopted for compatibility reasons, fully satisfies the accuracy requirements recommended for the reconstruction of the pathline (Benquè et al. 1982).

TEST CASES

To validate the code, we consider two typical situations that occur in river flow. These tests have been specifically designed to test the discretization of the nonlinear terms in the equations and the mass-conservation property of the numerical scheme. In addition, they are used to test for the presence of spurious oscillations arising due to the boundary conditions.

The first test is the simulation of a steady jet in a circular reservoir; the details of this classical test case as well as the experimental results can be found in Falconer (1980). The geometry of the boundary and the computational grid are shown in Fig. 2. We use an eddy coefficient $\mu = 2.5\ 10^{-4}\ m^2/s$ and a time step of 2 s. The computed velocity field is shown in Fig. 3. The solution slightly differs from the one shown in Benquè et al. (1982) and Falconer (1980); the location of the gyre centers is again sufficiently well described, but the maximum computed velocities in the gyres here fit better with the experimental ones. In particular, the cited references show an underestimation of the velocity in the region near the inflow, which is not present here. The reason of this is probably twofold: the quadratic representation of the discharge yields to a more accurate computation of the velocities and, above all, the use of an unstructured grid avoids the staircase boundary typical of finite-difference applications, so that the free-slip boundary conditions at the wall can be fulfilled here.

The second test case that we consider is the steady one-dimensional (1D) flow in a prismatic channel, without diffusion and bottom friction effects. Under these hypotheses SWE reduces to

$$\mathbf{q} = (Q, 0); \quad h = h(x) \tag{14}$$

$$\frac{d}{dx}\left(\frac{Q^2}{h}\right) + gh\frac{dh}{dx} = gh\frac{dh_0}{dx} \tag{15}$$

where Q = (constant) unit-width discharge. If the bottom field is defined as

$$h_0(x) = H + \gamma x - \frac{Q^2}{2g}\left[\frac{1}{H^2} - \frac{1}{(H+\gamma x)^2}\right] \tag{16}$$

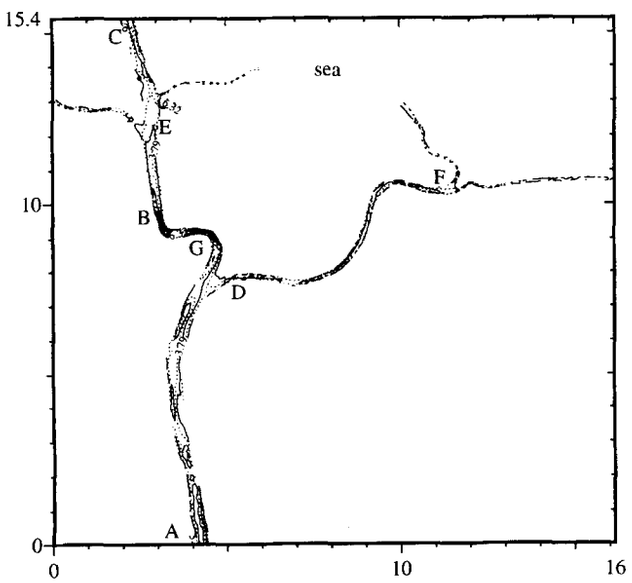

FIG. 6. Contour of Po River Delta

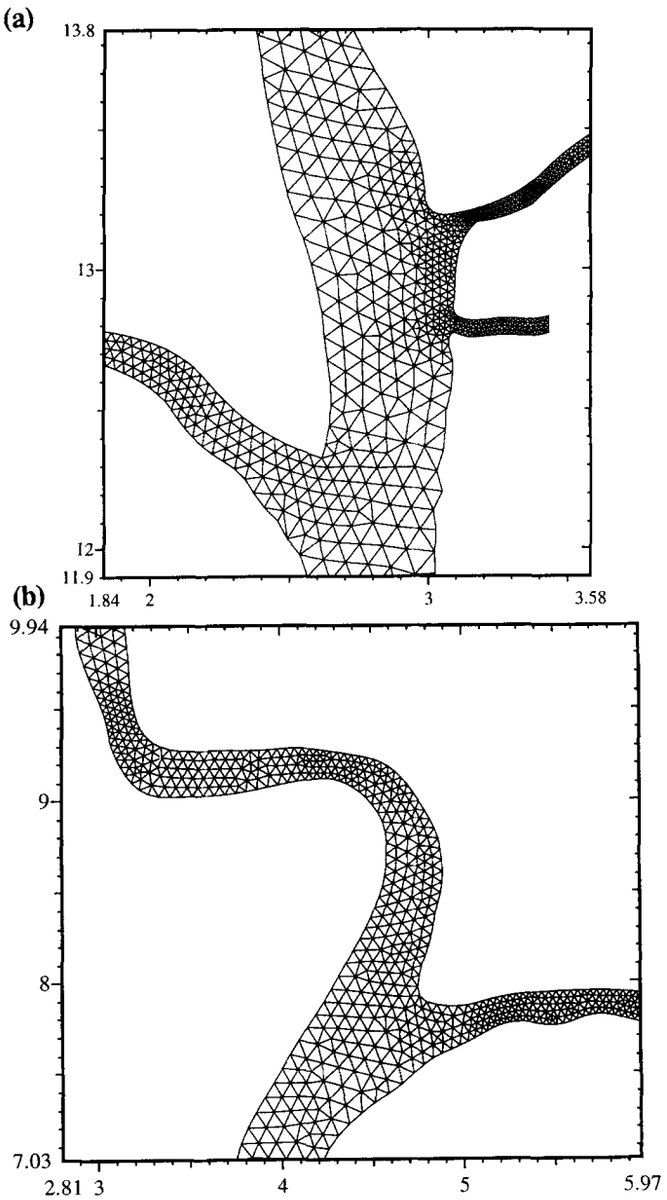

FIG. 7. Detail of Fine Mesh in Areas E and G

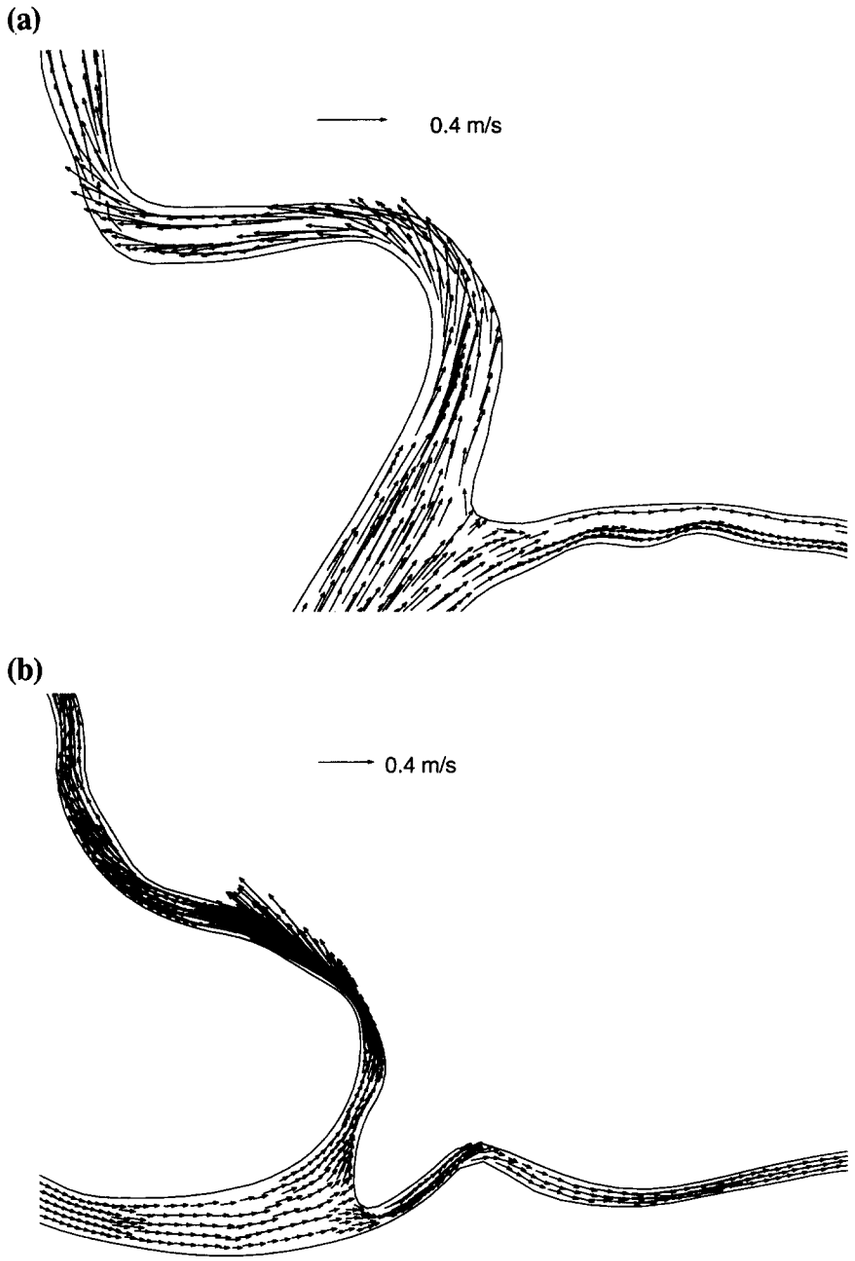

FIG. 8. Velocity Field in Areas G and F Computed on Coarse Mesh

where H and γ = constant values, it can be easily verified that (15) has the following exact solution:

$$h(x) = H + \gamma x; \quad q(x) = Q \tag{17}$$

This test case allows for the verification of the accuracy of the scheme when a strong gradient is present in the bathymetry, as often occurs in rivers.

The computation for this test has been carried out using an inflow depth $H = 4$, an inflow unit-width discharge $Q = 4$, and a bottom slope $\gamma = 0.06$. Although this test is essentially 1D, an analogous case for the 2D code has been run on a channel 300 m long and 4 m wide. The computational mesh is almost regular; it is composed by 580 elements, and a detail of it may be seen in Fig. 4.

For the boundary conditions, the value of Q has been imposed at the inflow, and the value of ξ has been imposed at the outflow. Fig. 5 contains two graphs: a plot of the exact elevation versus the computed elevation and a plot of the computed unit-width discharge. The former plot evidences the good accuracy of the scheme for the elevation as well as the fulfillment of the mass-conservation property with a small loss of 0.5% for this mesh.

It should be mentioned that a very large number of time steps were required to reach the steady-state solution, since no mechanism to dissipate the spurious components of the initial conditions is present in this computation.

DELTA OF PO RIVER

In the present study, we apply the numerical scheme previously described for the simulation of the flow at the delta of the Po River, i.e., the final 20 km of its length. A plot of the river contours together with a very rough description of the bottom may be seen in Fig. 6. In this map, the areas that are marked by letters denote regions where experimental measures are available or where the flow field has some particular features that will be discussed.

This final part of the Po River is characterized by an intricate pattern and a strongly varying bottom that make the nu-

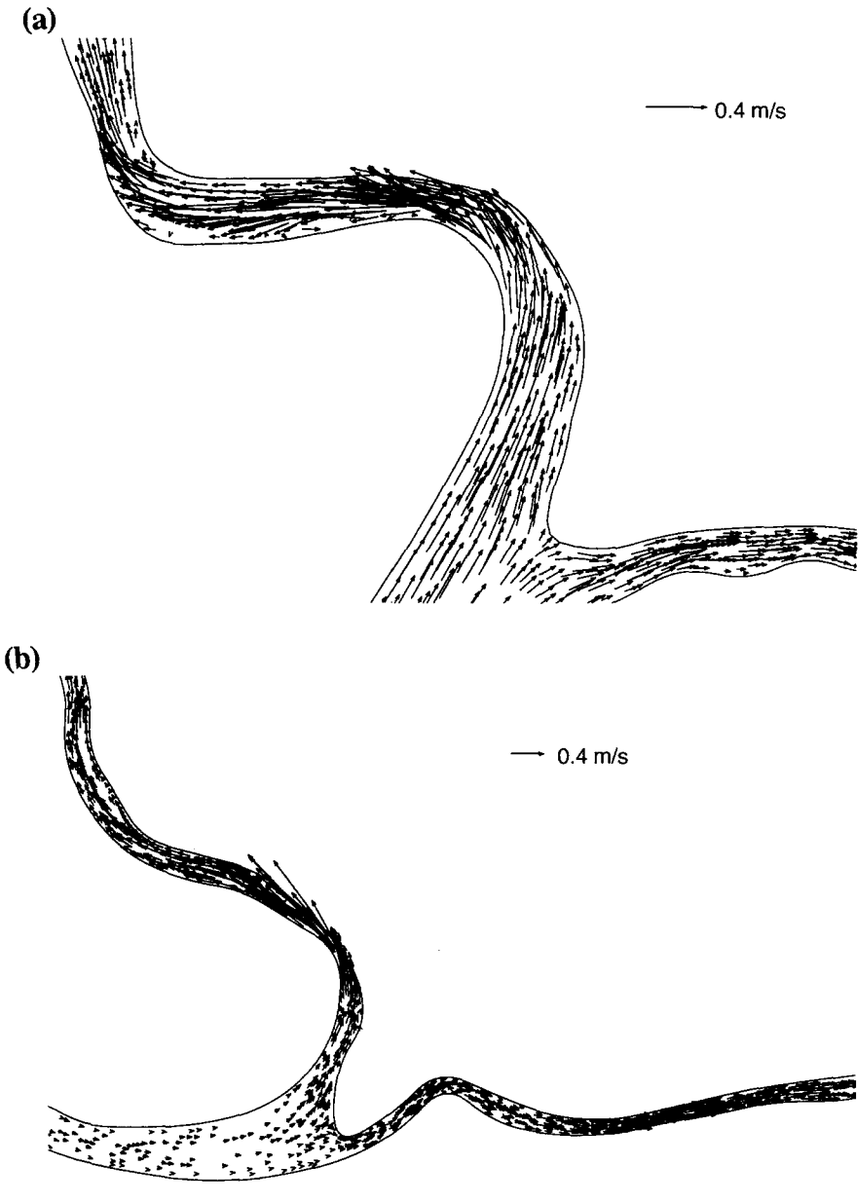

FIG. 9. Velocity Field in Areas G and F Computed on Fine Mesh

merical simulation of the flow nontrivial. The width of the river at the inflow is 379 m; the depth varies between a few centimeters and 17 m. Below the first bifurcation, the river has a narrow bend. Here the river width decreases, the depth strongly increases (area G of Fig. 6), and one expects the velocity $\mathbf{v}$ and especially the unit-width discharge $\mathbf{q}$ to assume large values and gradients.

The boundary conditions are chosen to fit our final task: the simulation of the flow evolution governed by the tidal-elevation variation corresponding to the experimental data available. Therefore, we impose the elevation everywhere at the open boundary and, if a boundary node is found to be of inflow type, the tangential velocity component is prescribed to be zero. No slip-boundary conditions have been used on the closed boundary.

Two computational meshes have been used: a coarse one with 3,185 elements and 2,172 vertices (with a minimum triangle diameter of 18 m) and a fine one with 10,602 elements and 6,481 vertices (with a minimum triangle diameter of 8 m). A detail of the fine mesh in two crucial areas may be seen in Fig. 7; the chosen regions correspond to those areas indicated by E and G in Fig. 6, respectively.

As a starting point for the simulations, we consider the solution of the steady-state flow field computed with the boundary conditions at the initial time used in the unsteady simulation. Considering the open river boundaries starting from the bottom in Fig. 6 and rotating in a counterclockwise sense, the imposed elevations for the steady-state computations are then 0.46, 0.35, 0.30, 0.41, 0.32, and 0.38 m.

NUMERICAL RESULTS

For the present computation, the Strickler coefficient has been set equal to 42 and the value of the viscosity coefficient is 0.1. A time step of 200 s has been used for the computations on the coarse mesh, and a time step of 100 s has been used for those on the fine mesh.

Figs. 8 and 9 show the velocity vectors computed by the code in two regions that have been indicated in the map by the letters G and F. For the sake of clarity, only a subset of the velocity vectors is plotted in these pictures.

The computed velocity field is subcritical everywhere with the largest Froude number in the whole domain being equal to 0.61. As would be expected, the velocity has strong gra-

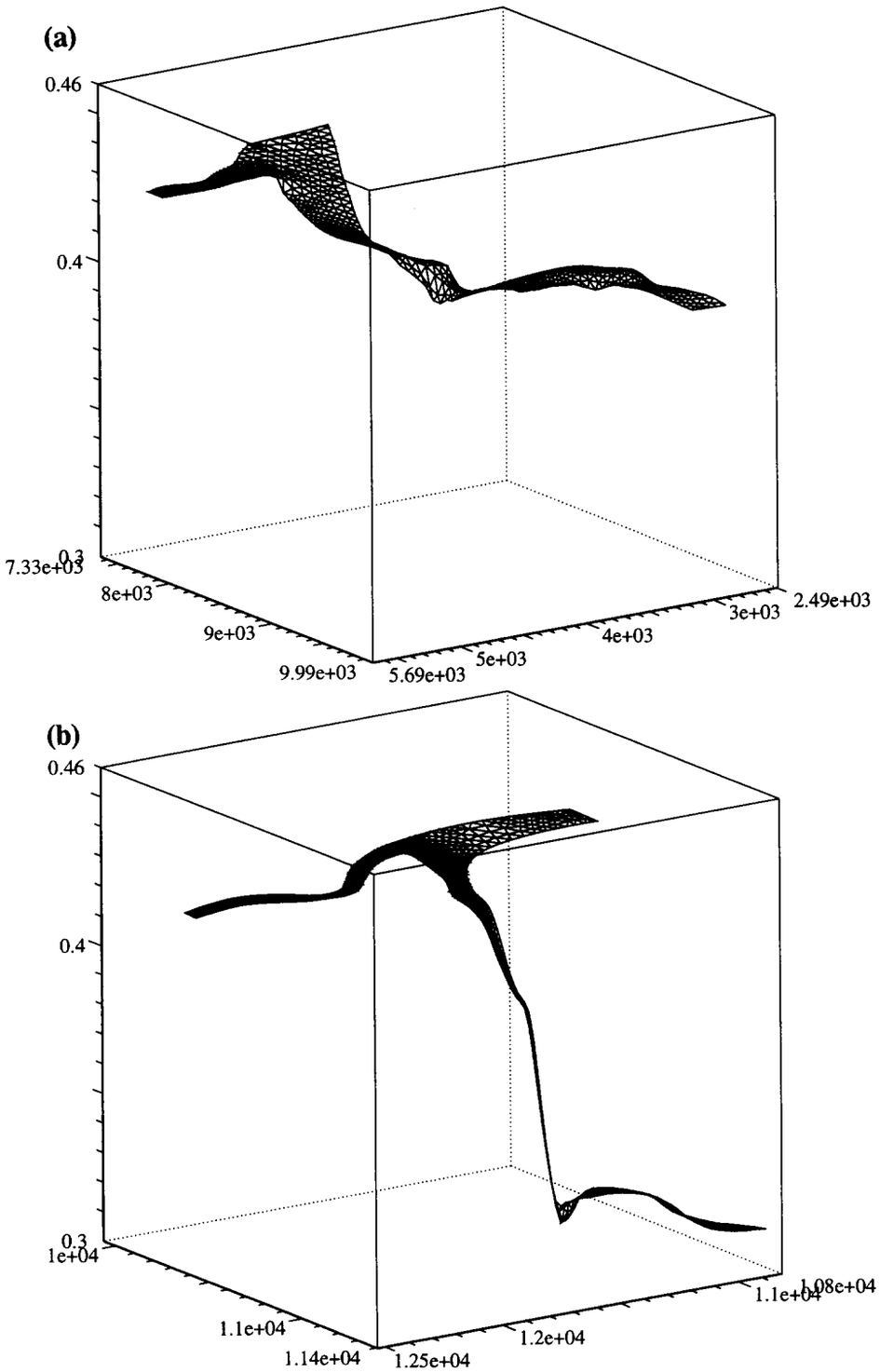

FIG. 10. Elevation of Water Level in Areas G and F

dients due to the simultaneous occurrence of three factors: the aspect ratio of the river is large, the bottom shows a strong variation, and the contour has a sharp elbow. In particular, in area G the bottom depth varies abruptly from 2 to 18 m, and in area F the river width collapses from 100 to 10 m. The meandering of the river makes the cross derivatives of the convective term (i.e., $v\ \partial u/\partial y$ and $u\ \partial v/\partial x$) dominant, which are of secondary importance when the river contour is straight. Therefore, an accurate treatment of the convection terms is necessary for the simulation of the local characteristics of the flow.

The velocity field resulting from the computation agrees with the preceding observations and confirms the good properties of stability and accuracy of the scheme. In fact, no oscillations appear neither in the velocity field and in the elevation, as may be seen in the 3D plot of Fig. 10. The velocity field computed on the fine mesh in Fig. 9 reveals two small recirculation zones that are not detected in the computation with the coarse mesh. The effects of inertia are also detectable by noting the variation of the velocity strength across the river section below a bend. However, these differences between the coarse and fine mesh occur on a local scale and do not affect

the total discharge at open boundaries, which is equally well computed by using both meshes.

The numerical simulation of the river flow over three days has been carried out using the same computational parameters as those previously specified and by imposing the experimental values of the elevation at the open boundary that evolve in time. The maximum amplitude of the tidal waves at the river outflow is 63 cm, which is a typical Mediterranean value. The results of the computation obtained by using the two meshes do not present relevant differences at the nodes where experimental measures are available; therefore, only the results relative to the coarse mesh will be shown. With reference to the computational cost, 50 min on a HP730 have been necessary to simulate three days of real flow.

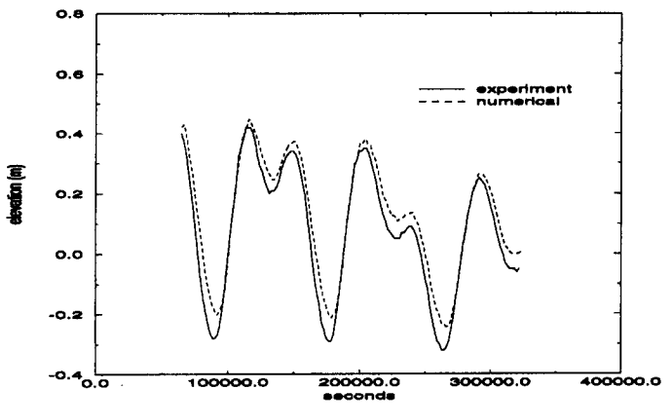

FIG. 11. Experimental and Numerical Values of Elevation in D

In Fig. 11, the computed and experimental elevation values on point D are plotted. The two curves agree rather well; the discrepancies are probably not due to the numerical method, as a very similar behavior has also been found using completely different approaches [as discussed in Ambrosi et al. (1994)].

Figs. 12 and 13 compare numerical and experimental results for the magnitude of the unit-width discharge vector corresponding to points located in the areas B, C, and A, respectively. Note that the curve between t = 95,000 s and t = 115,000 s for these plots is relative to the upstream flow. When comparing the numerical and experimental data, one should take into account the following two observations. First, the experimental velocity measures may be inaccurate due to small variations of the position where the measurement occurred. Second, the computational results are strongly dependent on the calibration of the Strickler coefficient, which in our sim-

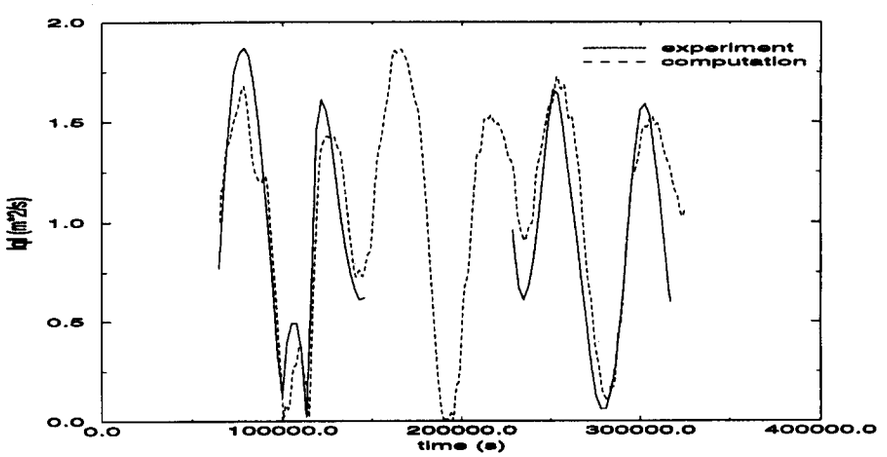

FIG. 12. Experimental and Numerical Values of Unit-Width Discharge in B

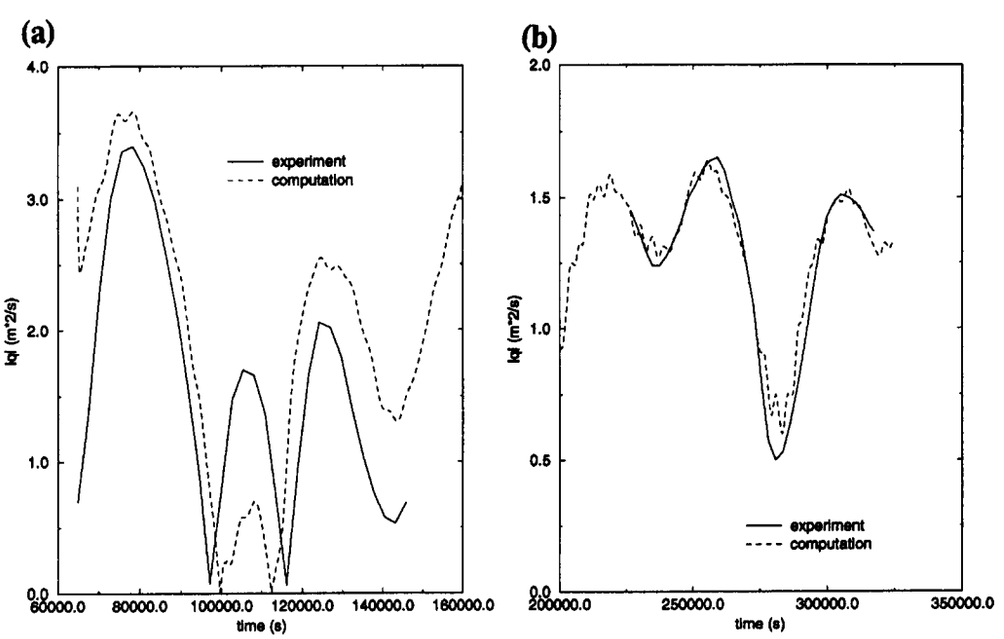

FIG. 13. Experimental and Numerical Values of Unit-Width Discharge in C and A

ulation has been set ad hoc to fit the measured discharge in the steady-state calculations. The diagrams for the area of inflow (A) and for the middle of the considered domain (B) show a satisfactory agreement between computational and experimental results. On the other hand, the diagram for the area of outflow (C) shows large discrepancies. This fact is particularly disappointing because the greater difference occurs in the region where the current is upstream, in particular for the nodes nearer to the sea where the prediction of salted water flow is most interesting from an engineering point of view. However, one of the possible explanations for this effect is that SWE in (1) and (2) assumes that density is constant; however, in reality, in region C fresh and salted water are present so that the measured density is variable as a function of the salinity. Therefore in such a region, a more realistic model should take into account the dynamics of the salinity field so that the water density becomes a variable dependent on space.

CONCLUSIONS

A finite-element method for the shallow-water equations has been presented and has been preliminarily tested in two simple geometries. The code has then been applied to the simulation of the flow of the Po River at the delta, carrying out a comparison between the numerical results and the experimental measures. The following remarks arise.

The geometrical flexibility ensured by a finite-element approach has been extremely useful in handling the complicated geometry of the Po River.

The use of the Lagrangian step allows an accurate and efficient integration of the convective terms. The fractional-step method used to advance in time ensures efficiency and unconditional stability at a low computational cost. When there are river bends (as in a present case), the role of inertia is visible in the results, and the use of a fine enough mesh reveals recirculation zones.

The use of a P1-P2 representation is known to be necessary to avoid spurious oscillations in the elevation. Here it is coupled with a Lagrangian discretization of the convective terms and a fractional-step time-advancing scheme that also eliminates any oscillations in the velocity.

The computational cost of this approach is very competitive, requiring only one hour to compute a real-life unsteady flow in a complicated geometry over three days.

The comparison with experimental results is rather satisfactory in regions sufficiently far from the mouths; near to the shoreline a more accurate physical model is probably necessary, and will be addressed in future.

ACKNOWLEDGMENTS

We are indebted to A. Balzano, D. Lorenzato, L. Trotta, and A. Quarteroni for many fruitful discussions. This work has been supported by ENEL-CRIS and by the Sardinian Regional Authorities.

APPENDIX. REFERENCES

Agoshkov, V. I., Ambrosi, D., Pennati, V., Quarteroni, A., and Saleri, F. (1993). "Mathematical and numerical modelling of shallow water flow. *Computational Mech.*, 11, 280–299.

Ambrosi, D., Corti, S., Pennati, V., and Saleri, F. (1994). "A 2D numerical simulation of the Po river delta flow." *Modelling of flood propagation over initially dry areas*, P. Molinaro and L. Natale, eds., ASCE, New York, N.Y., 18–25.

Benquè, J. P., Cunge, J. A., Feuillet, J., Hauguel, A., and Holly, F. M. (1982). "New method for tidal current computation." *J. Wtrwy., Port, Coast., and Oc. Div.*, ASCE, 108, 396–417.

Cunge, J. A., Holly Jr., F. M., and Verwey, A. (1981). *Practical aspects of computational river hydraulics*. Pitman Publishing, Ltd., London, England.

Di Monaco, A., and Molinaro, P. (1988). "A finite-element two-dimensional model of free surface flow: verification against experimental data for the problem of emptying of a reservoir due to dam-breaking." *Proc., 1st Int. Conf. on Comp. Methods and Water Res.*, 2, 301–312.

Falconer, R. A. (1980). "Numerical modeling of tidal circulation in harbors." *J. Wtrwy., Port, Coast., and Oc. Div.*, ASCE, 106(1), 31–48.

Leclerc, M., Bellemare, J. F., Dumas, G., and Dhatt, G. (1990). "A finite element method of estuarian and river flows with moving boundaries." *Adv. Water Resour.*, 13(4), 158–168.

Lynch, D. R., and Gray, W. G. (1979). "A wave equation model for finite element tidal computations." *Comp. and Fluids*, 7, 207–228.

Oliger, J., and Sundstrom, A. (1978). "Theoretical and practical aspects of some initial boundary value problems in fluid dynamics." *SIAM J. Appl. Mathematics*, 35(3), 419–445.

Pironneau, O. (1982). "On the transport-diffusion algorithm and its application to the Navier-Stokes equations." *Numerische Matematik*, 38, 309–332.

Quarteroni, A., and Valli, A. (1994). *Numerical approximation of partial differential equations*. Springer-Verlag New York, Inc., New York, N.Y.

Walters, A. (1983). "Numerically induced oscillations in the finite element approximations to the shallow water equations." *Int. J. Numer. Methods in Fluids*, 3, 591–604.

Westerink, J. J., Luettich Jr., R. A., Wu, J. K., and Kolar, R. L. (1994). "The influence of normal flow boundary conditions on spurious modes in finite element solutions to the shallow water equations." *Int. J. Numer. Methods in Fluids*, 18, 1021–1060.

Zienkiewikz, O. C., and Taylor, R. L. (1989). *The finite element method*. McGraw-Hill Book Co., Inc., New York, N.Y.